

Supplementary Materials

High-Performance Sub-10 nm Monolayer Bi₂O₂Se Transistors

Ruge Quhe,^{1,*} Junchen Liu,¹ Jinxiong Wu,³ Jie Yang,² Yangyang Wang,⁵ Qiuuhui Li,¹ Tianran Li,³ Ying Guo,⁶ Jinbo Yang,^{2,4} Hailin Peng,³ Ming Lei,^{1,*} and Jing Lu^{2,4,*}

¹ State Key Laboratory of Information Photonics and Optical Communications, Beijing University of Posts and Telecommunications, Beijing 100876, P. R. China

² State Key Laboratory for Mesoscopic Physics and Department of Physics, Peking University, Beijing 100871, P. R. China

³ Center for Nanochemistry, Beijing National Laboratory for Molecular Sciences (BNLMS), College of Chemistry and Molecular Engineering, Peking University, Beijing 100871, P. R. China

⁴ Collaborative Innovation Center of Quantum Matter, Beijing 100871, P. R. China

⁵ Nanophotonics and Optoelectronics Research Center, Qian Xuesen Laboratory of Space Technology, China Academy of Space Technology, Beijing 100094, P. R. China

⁶ School of Physics and Telecommunication Engineering and Shaanxi Key Laboratory of Catalysis, Shaanxi University of Technology, Hanzhong 723001, P. R. China

*Corresponding author: jinglu@pku.edu.cn; mlei@bupt.edu.cn; quheruge@bupt.edu.cn

Table S1. Benchmark of the ballistic performance upper limits of the ML Bi₂O₂Se MOSFETs against the ITRS 2.0 2013 edition requirements for HP devices.

	<i>L_g</i> (nm)	EOT (nm)	V _{dd} (V)	UL (nm)	I _{on} (μA/μm)	C _{total} (fF/μm)	τ (ps)	PDP (fJ/μm)
				0	—	0.06	—	0.025
<i>n</i> -type				2	0.2	0.06	183	0.025
	1.0	0.41	0.64	4	130	0.03	0.261	0.012
				0	0.6	0.09	117	0.037
<i>p</i> -type				2	67	0.09	0.522	0.037
				4	296	0.06	0.099	0.025
				0	—	0.15	—	0.061
<i>n</i> -type				2	1.7	0.15	51	0.061
	2.0	0.41	0.64	4	871	0.09	0.072	0.037
				0	2.3	0.15	42	0.061
<i>p</i> -type				2	470	0.12	0.180	0.049
				4	569	0.15	0.165	0.061
				0	—	0.21	—	0.086
<i>n</i> -type				2	285	0.12	0.267	0.049
	3.0	0.41	0.64	3	996	0.15	0.093	0.061
<i>p</i> -type				0	52	0.18	2.334	0.074
				2	1127	0.27	0.102	0.111
<i>n</i> -type				0	306	0.36	0.762	0.147
	5.0	0.41	0.64	2	2067	0.30	0.093	0.123
<i>p</i> -type				0	1147	0.39	0.219	0.160
ITRS HP 2028	5.1				900	0.60	0.423	0.240
<i>n</i> -type				0	2126	0.39	0.126	0.180
<i>p</i> -type	6.7	0.47	0.68	0	1840	0.54	0.204	0.250
ITRS HP 2025					1100	0.77	0.451	0.360
<i>n</i> -type				0	3380	0.48	0.102	0.249
<i>p</i> -type	8.8	0.54	0.72	0	1819	0.72	0.285	0.373
ITRS HP 2022					1350	0.87	0.463	0.450

Table S2. Benchmark of the ballistic performance upper limits of the ML Bi₂O₂Se MOSFETs against the ITRS 2.0 2013 edition requirements for LP devices.

	L_g (nm)	EOT (nm)	V_{dd} (V)	UL (nm)	I_{on} ($\mu\text{A}/\mu\text{m}$)	C_{total} (fF/μm)	τ (ps)	PDP (fJ/μm)
				0	–	0.12	–	0.049
<i>n</i> -type				2	–	0.15	–	0.061
	1.0	0.41	0.64	4	–	0.15	–	0.061
				0	–	0.06	–	0.025
<i>p</i> -type				2	–	0.12	–	0.049
				4	0.4	0.09	144	0.037
				0	–	3.00	–	1.229
<i>n</i> -type				2	–	3.00	–	1.229
	2.0	0.41	0.64	4	–	0.30	–	0.123
				0	–	0.21	–	0.086
<i>p</i> -type				2	3.8×10^{-3}	0.21	3.5×10^4	0.086
				4	46.8	0.06	0.821	0.025
<i>n</i> -type				0	–	0.42	–	0.172
	3.0	0.41	0.64	2	–	0.45	–	0.184
<i>p</i> -type				0	6.1×10^{-4}	0.33	3.5×10^5	0.135
				2	1.7	0.09	34	0.037
<i>n</i> -type				0	–	0.63	–	0.258
	5.0	0.41	0.64	2	4.1×10^{-3}	0.63	9.8×10^4	0.258
<i>p</i> -type				0	0.2	0.39	1.2×10^3	0.160
				2	2.9	0.24	53	0.098
ITRS LP 2028	5.9				295	0.69	1.493	0.280
<i>n</i> -type				0	3.8×10^{-3}	0.78	1.4×10^5	0.340
<i>p</i> -type	7.0	0.45	0.66	0	411	0.42	0.674	0.183
ITRS LP 2026					337	0.77	1.514	0.340
<i>n</i> -type				0	10	0.81	57.5	0.408
<i>p</i> -type	9.3	0.51	0.71	0	830	0.45	0.385	0.227
ITRS LP 2023					458	0.95	1.474	0.480

Table S3. Benchmark of the ballistic performance upper limits of the ML MoS₂ MOSFETs against the ITRS 2.0 2013 edition requirements for HP devices.

	L_g (nm)	UL (nm)	EOT (nm)	V_{dd} (V)	I_{on} (μA/μm)	C_{total} (fF/μm)	τ (ps)	PDP (fJ/μm)
		0			4	0.11	17.280	0.015
<i>n</i> -type		2			61	0.11	1.102	0.015
	1	4	0.41	0.64	113	0.10	0.578	0.014
		0			34	0.10	1.864	0.014
<i>p</i> -type		2			293	0.09	0.190	0.012
		4			283	0.07	0.149	0.009
		0			216	0.63	1.867	0.086
<i>n</i> -type	5	2		0.64	230	0.56	1.544	0.076
		0	0.41		519	0.45	0.555	0.061
<i>p</i> -type		2			598	0.32	0.344	0.044
ITRS HP 2028	5.1			0.68	900	0.60	0.423	0.240
<i>n</i> -type	9	0		0.64	230	1.26	3.506	0.172
<i>p</i> -type			0.51		510	0.84	1.054	0.115
ITRS HP 2022	8.8			0.72	1350	0.87	0.463	0.450

Table S4. Simulation parameters of the sub-10 nm MOSFETs. All the devices are simulated at the DFT+NEGF level and double gate configurations. The source and drain are degenerately doped with the doping concentration ρ .

	channel material	basis set	V_{dd} (V)	ρ (cm^{-2})
<i>n</i> -type	$\text{Bi}_2\text{O}_2\text{Se}$	DZP	0.64 – 0.72	5×10^{13}
	MoS_2	DZP	0.64	5×10^{13}
	InSe	DZP	0.64	1×10^{13}
	Arsenene	DZP	0.64 – 0.72	$(1–5) \times 10^{13}$
	Antimonene	DZP	0.64	1×10^{13}
<i>p</i> -type	$\text{Bi}_2\text{O}_2\text{Se}$	DZP	0.64 – 0.72	5×10^{13}
	MoS_2	DZP	0.64	5×10^{13}
	InSe	DZP	0.64	9×10^{13}
	Phosphorene	SZP	0.69 – 0.78	4×10^{13}

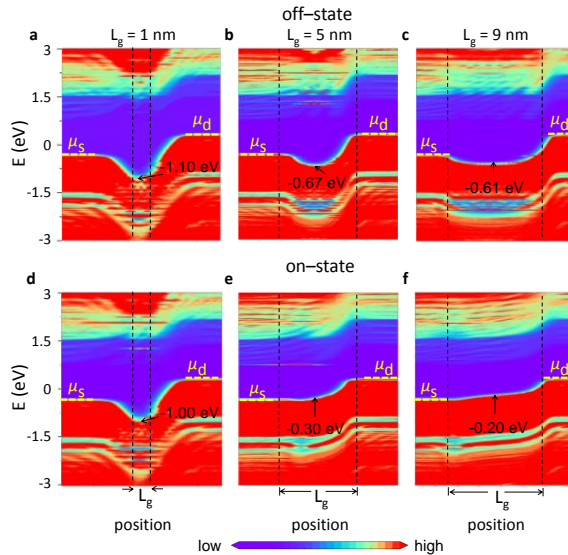


Fig. S1. Comparison of the local density of states of the ML $\text{Bi}_2\text{O}_2\text{Se}$ *p*-MOSFETs at the off- and on-states with different gate length. UL = 0 nm. μ_s and μ_d are the electrochemical potential of the source and drain, respectively. The off-state has a current of 0.1 $\mu\text{A}/\mu\text{m}$, and the on-state is the state with a gate difference of $V_{dd} = 0.64$ V to the off-state. The energy of VBM at the middle of the channel (E_{mid}) is labeled.

The comparison of the local density of states of the ML $\text{Bi}_2\text{O}_2\text{Se}$ *p*-MOSFETs with different gate lengths is shown in Fig. S1. To evaluate the modulation of the band edge location by gate voltage, the energy of the valence band edge at the middle of the channel (E_{mid}) is labeled. No UL is considered in this comparison. To achieve the current of 0.1 $\mu\text{A}/\mu\text{m}$ at the off-state, E_{mid} at $L_g = 1$ nm is the lowest, followed by those at $L_g = 5$ nm and 9 nm. With a gate voltage

variation of 0.64 V, the changes of E_{mid} at $L_g = 1$ nm, 5 nm and 9 nm are 0.10 eV, 0.37 eV and 0.41 eV, respectively. The enhanced modulation of E_{mid} suggests the improved gate controllability and this trend is consistent with smaller SS at longer L_g .

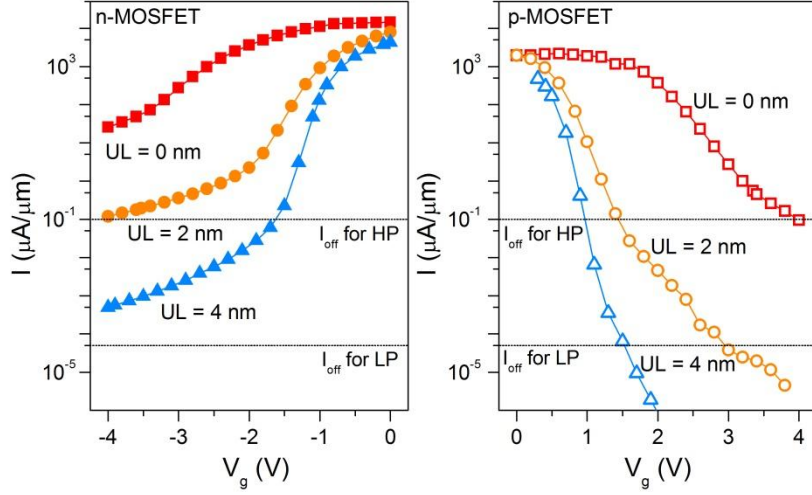


Fig. S2. Transfer characteristics of the ML $\text{Bi}_2\text{O}_2\text{Se}$ MOSFETs with different underlaps. $L_g = 1$ nm. The supply voltage is set to 0.64 V.

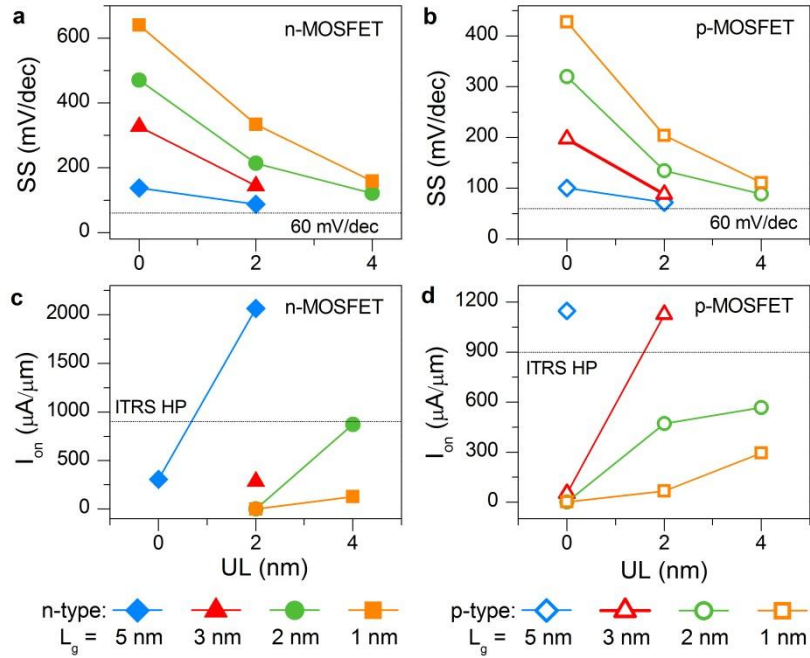


Fig. S3. SS and on-current of the ML $\text{Bi}_2\text{O}_2\text{Se}$ MOSFETs as a function of UL. The supply voltage is set to 0.64 V.

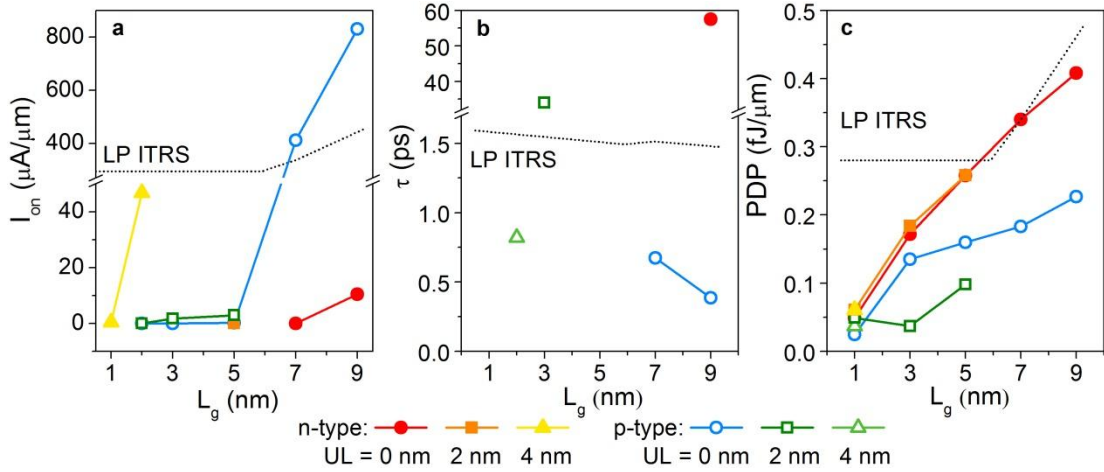


Fig. S4. On-current, delay time and power dissipation of the ML $\text{Bi}_2\text{O}_2\text{Se}$ MOSFETs as a function of the gate length for LP applications. $V_{dd} = 0.64 \sim 0.71$ V.

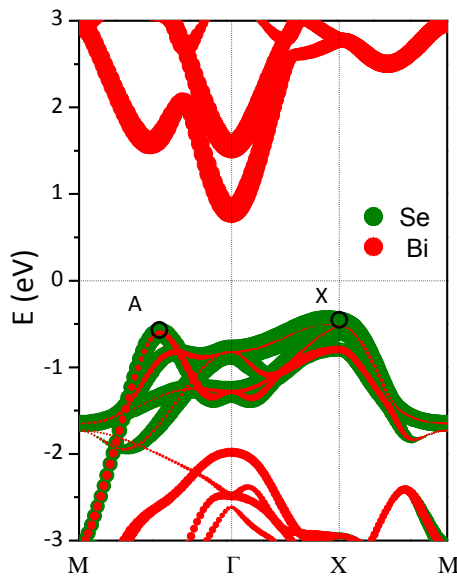


Fig. S5. Band structure of ML $\text{Bi}_2\text{O}_2\text{Se}$ calculated by using the plane wave basis set and projector augmented wave (PAW) potential, as implemented in the VASP code. The green and red points stand for the contributions from Se and Bi atoms, respectively, and the size of the points is proportional to the contribution weight.

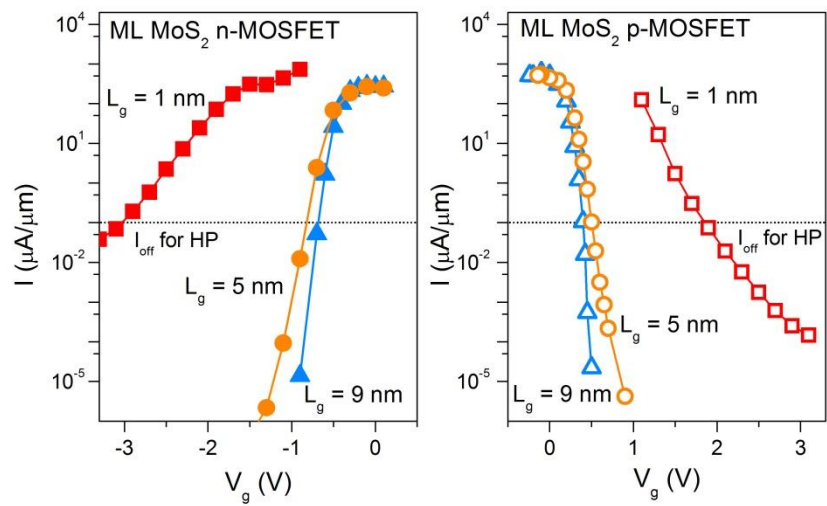


Fig. S6. Transfer characteristics of the ML MoS_2 MOSFETs with different gate length. UL = 0 nm. The supply voltage is set to 0.64 V.